EUROPEAN ORGANIZATION FOR NUCLEAR RESEARCH

CERN-EP/79-86
30 July 1979

A PARTIAL WAVE ANALYSIS OF THE $p\bar{p}$ SYSTEM PRODUCED AT LOW FOUR-MOMENTUM TRANSFER IN THE REACTION $\pi^- p \to p\bar{p}n$ AT 18 GeV

M. Rozanska*), W. Blum, H. Dietl, G. Grayer**), E. Lorenz,
G. Lütjens, W. Männer, J. Meissburger***),
R. Richter and U. Stierlin

Max-Planck Institute, Munich, Germany

V. Chabaud, B. Hyams, K. Rybicki*) and P. Weilhammer

CERN, Geneva, Switzerland

ABSTRACT

Results of an analysis of two high statistic samples of $p\bar{p}$ events (10,700 events at p_{lab} = 18.8 GeV and 35,000 events at p_{lab} = 18.4 GeV) are presented. The data extend from threshold to 2.8 GeV invariant mass. The production proceeds dominantly via one-pion exchange with absorption corrections. The mass spectrum and decay angular distribution can be explained as a superposition of resonating partial waves with spin J = 2, 3, 4, 5. Indications of a spin 6 state at 2.71 GeV are found.

(Submitted to Nuclear Physics B)

---

*) Permanent address: Institute of Nuclear Physics, Krakow, Poland.

**) Now at the Rutherford Laboratory, Chilton, Didcot, Oxon, England.

***) Now at the Kernforschungsanlage, Jülich, Germany.

1. INTRODUCTION

We present an analysis of resonant states produced in the $p\bar{p}$ system. The $p\bar{p}$ pairs were peripherally produced in the reaction:

$$\pi^- p \to p\bar{p}n \ . \qquad \text{(a)}$$

The production of resonances on the leading trajectory is expected to be suppressed in the $p\bar{p}$ system by centrifugal barrier effects. Therefore reaction (a) is better suited for the investigation of high mass and low-spin meson resonances than pion or kaon pair production. These resonances are expected by various models to lie on the daughter meson trajectories (see, for example, Hey and Morgan [1]).

A partial wave analysis of the $p\bar{p}$ system produced in reaction (a) was previously performed by this group with only the sample measured at 18.8 GeV, assuming a pure one-pion exchange as a production mechanism [2,3]. Most of the information on the $p\bar{p}$ system comes from studying specific two-body channels in $p\bar{p}$ formation experiments (see, for example, Eisenhandler et al. [4], Carter et al. [5]), in particular:

$$p\bar{p} \to \pi^+\pi^- \ . \qquad \text{(b)}$$

An analysis of the differential cross-sections is highly model-dependent; however, it seems possible to establish a sequence of resonances with spin parity $J^{PC} = 3^{--}, 4^{++}, 5^{--}$.

2. THE DATA

The reaction (a) was measured in two spark chamber experiments at 18.8 GeV and 18.4 GeV primary momenta (c omitted in all dimensions). The apparatus was designed for the study of peripheral production of quasi-two-body reactions. The $p\bar{p}$ final state was selected with two atmospheric pressure gas Čerenkov counters suppressing π and K pairs. The neutron was not observed but identified in a 1C fit. Table 1 lists the numbers of events and background contributions.

Further details of the apparatus, selection criteria, and data treatment are given elsewhere [2,3,6].

Figure 1 shows the observed and corrected spectrum of $p\bar{p}$ effective mass M. The final spectrum has been corrected for geometric acceptance as well as for various geometry-independent losses. The acceptance correction was calculated by randomly rotating the observed events around their beam particle direction. Small variations due to beam energy spread and the vertex distribution, etc., were also taken into account. The cross-section for one event in the corrected mass spectrum corresponds to:

$$\sigma(1 \text{ event}) = 0.08 \pm 0.01 \text{ nb} .$$

Our analysis has been performed in the $p\bar{p}$ effective mass range from 1.975 to 2.75 GeV and a four-momentum transfer t from the initial proton to the neutron of less than 0.3 GeV^2 (t was defined to be positive in the physical region). In this region the acceptance varies between 30% and 98% and is non-zero in the full range of decay angles of the $p\bar{p}$ system. Figure 2 shows the acceptance for an isotropically decaying $p\bar{p}$ system as a function of its effective mass for several values of the four-momentum transfer t. The mass resolution σ varied from 2 MeV for M = 1.95 GeV up to 8 MeV for M = 2.75 GeV.

3. PRODUCTION MECHANISMS

An inspection of differential cross-sections indicates that for t below 0.3 GeV^2 $p\bar{p}$ pairs are predominantly produced by a one-pion exchange mechanism (OPE) with a small background contribution.

Figure 3 shows the corrected differential cross-sections $d\sigma/dt$ measured at 18.8 GeV for a few mass bins compared with predictions of the OPE model of ref. [7]. According to this model, the t-dependence of the differential cross-section of the OPE process can be described by the Born-term amplitude multiplied by kinematical form factors:

$$\frac{d\sigma}{dt} \sim \frac{t}{(t + m_\pi^2)^2} F_1(t) F_2(t) . \qquad (1)$$

The form factors $F_1(t)$ and $F_2(t)$ provide off-shell vertex correction. For the $p\pi^+n$ vertex the following phenomenological Dürr-Pilkuhn nucleon vertex form factor [8] was used:

$$F_1(t) \equiv F_{DP}(t) = (1 + R^2Q^2)/(1 + R^2Q_t^2) \ , \qquad (2)$$

where

$Q_t^2 \approx t(4m_p^2 + t)/4m_p^2$

$Q^2 = Q_t^2(t = -m_\pi^2)$

$R = 2.86 \pm 0.08$ GeV^{-1} (see ref [7]).

Because of high mass values at the second vertex ($M \geq 2m_p$), the form factor $F_2(t)$ was set to unity. Except for masses below 2 GeV, the shape of $d\sigma/dt$ is correctly reproduced up to $t = 0.3$ GeV^2.

If reaction (a) is dominated by OPE, the Chew-Low formula [9] and detailed balance can be used to predict the $p\bar{p}$ mass spectrum in this reaction from results of $p\bar{p} \to \pi^+\pi^-$ formation experiments. The original Chew-Low formula was modified by the Dürr-Pilkuhn nucleon vertex form factor:

$$\frac{\Delta N}{\Delta M} = \frac{1}{\sigma(1 \text{ event})} \frac{1}{4\pi m_p^2 p_{lab}^2} \frac{G^2}{4\pi} \int_{\Delta M} dM \int_{t_{min}}^{t_{max}} dt \, \frac{t}{(t + m_\pi^2)^2} F_{DP}(t) q^* M^2 \sigma(M)_{\pi^+\pi^- \to p\bar{p}} \qquad (3)$$

where

m_p, m_π are the proton and pion masses, respectively,

$q^* = \left(\left[t^2 + 2t(m_\pi^2 + M^2) + (m_\pi^2 - M^2)^2 \right]/4M^2 \right)^{1/2}$, and

$G^2/4\pi = 29.2 \, ^{+\ 1.0}_{-\ 1.4}$ is the $p\pi^+n$ coupling constant.

The cross-sections $\sigma_{\pi^+\pi^- \to p\bar{p}}$ in eq. (3) are obtained from cross-sections for annihilation $\sigma_{p\bar{p} \to \pi^+\pi^-}$ using the detailed balance relation:

$$\sigma(M)_{\pi^+\pi^- \to p\bar{p}} = \frac{(2S_p + 1)(2S_{\bar{p}} + 1)}{(2S_{\pi^+} + 1)(2S_{\pi^-} + 1)} \left(\frac{q_p}{q_\pi} \right)^2 \sigma(M)_{p\bar{p} \to \pi^+\pi^-} \qquad (4)$$

where

q_p, q_π are proton and pion momenta in the c.m. frame, and

$S_p = S_{\bar{p}} = 1/2$, and $S_{\pi^+} = S_{\pi^-} = 0$ are the spins of p, $\bar{p}$, and π^+, π^-, respectively.

Figure 1 shows the $p\bar{p}$ mass spectrum measured in reaction (a), averaged over the t inverval from t_{min} to 0.3 GeV^2. The data are compared with predictions from

the recent results of $p\bar{p} \to \pi^+\pi^-$ experiments [4,5]. The errors are only statistical. We observe an excellent agreement. The small systematic differences can be explained by uncertainties in the over-all cross-section normalization (typically 10%) and uncertainties in the acceptance corrections.

Furthermore, one can study the decay angular distribution and compare it with the results of reaction (b).

It is convenient to decompose the $p\bar{p}$ angular distribution into moments $\langle Y_\mu^L \rangle$, i.e. express the differential cross-section in the following form:

$$\frac{d^4\sigma}{dtdM\ \cos\theta\ d\phi} = \sum_L \sum_{\mu=-L}^{L} \langle Y_\mu^L \rangle \ \mathrm{Re}\ Y_\mu^L(\theta,\phi)\ \frac{d^2\sigma}{dtdM} \ . \tag{5}$$

The moments $\langle Y_\mu^L \rangle$ are functions of t and M. For the pure OPE process all moments $\langle Y_{\mu\neq 0}^L \rangle$ should vanish in the Gottfried-Jackson (GJ) frame. All moments $\langle Y_\mu^L \rangle$ measured in reaction (a) are compatible with zero for $\mu \geq 2$ for $t < 0.3\ \mathrm{GeV}^2$. The moments $\langle Y_1^L \rangle$ are very small compared with the $\langle Y_0^L \rangle$ moments. However, they show systematic structure which, as a function of the $p\bar{p}$ mass, is a mirror image of the structure observed in the $\langle Y_0^L \rangle$ moments (figs. 4-6). The ratio $\langle Y_1^L \rangle / \langle Y_0^L \rangle$ takes small negative values and in general represents a smooth continuation of the behaviour observed for lower masses in the reactions

$$\pi^- p \to \pi^+\pi^- n \tag{c}$$

$$\pi^- p \to K^+K^- n \ . \tag{d}$$

In particular, the absolute value of $\langle Y_1^L \rangle / \langle Y_0^L \rangle$ is decreasing as a function of mass [6,10].

It should be noted that in the previous analysis of reaction (a) [2,3] a much smaller sample was used. There the statistical error completely obscured the small structure in the $\langle Y_1^L \rangle$ moments; thus it was justifiable to set them to zero.

Non-vanishing $\langle Y_1^L \rangle$ moments indicate that the $p\bar{p}$ system is also produced in a helicity $\mu = \pm 1$ state. The contribution of amplitudes for the production of these states to the cross-sections integrated over angular variables is negligible,

but they can produce significant effects in angular distributions. In order to compare angular distributions in the Gottfried-Jackson angle with angular distributions of reaction (b), the curves $d\sigma/d\cos\theta$ were recalculated from the $\langle Y_0^L \rangle$ moments, measured in reaction (a). We expect that the contribution of amplitudes with helicity $\mu \neq 0$ to these moments can be neglected. The curves are shown in fig. 7 and compared with the angular distributions measured in $p\bar{p} \to \pi^+\pi^-$ experiments [5]. The curves are normalized using again the Chew-Low equation and detailed balance. We observe a good agreement in the absolute amount and the shape of $d\sigma/d\cos\theta$, except around $\cos\theta = \pm 1$. Discrepancies in this $\cos\theta$ region can be attributed to measurement errors and can explain systematic differences between $\langle Y_0^L \rangle$ moments obtained in reactions (a) and (b) [2]. It should be noted that the acceptance shows a rapid variation around $\cos\theta = \pm 1$. In the experiment $p\bar{p} \to \pi\pi$ [5], the data are only displayed below $|\cos\theta| < 0.98$. In our experiment, the acceptance has normally a local minimum around $|\cos\theta| \approx 0.95$ and rises to $\approx 100\%$ at $|\cos\theta| = 1$.

5. AMPLITUDE ANALYSIS

In order to describe reaction (a) we use the following set of assignments and variables:

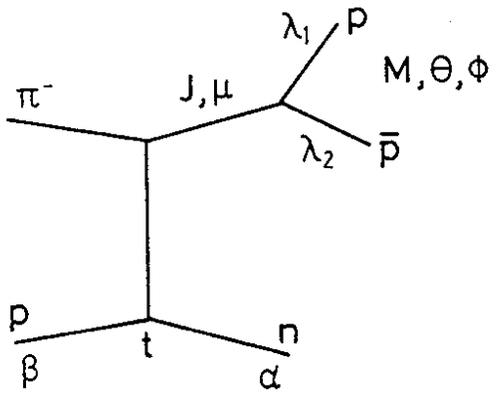

where

J, μ are the total spin and helicity of the $p\bar{p}$ system,

λ_1, λ_2 are the helicities of the proton and antiproton, respectively,

θ, ϕ are the decay angles of $\bar{p}$ in the GJ reference frame,

β, α are the helicities of the incident proton and neutron, respectively,

$q^* = \sqrt{M^2/4 - m_\pi^2}$ which is the π^+, π^- momentum in the $p\bar{p}$ rest frame,

$q = \sqrt{M^2/4 - m_p^2}$ which is the p, $\bar{p}$ momentum in the $p\bar{p}$ rest frame.

The differential cross-sections for reaction (a) can be expressed as:

$$\frac{d^4\sigma}{dt\,dM\,d\cos\theta\,d\phi} = C \sum_{\alpha,\beta,\lambda_1,\lambda_2} |A_{\alpha\beta\lambda_1\lambda_2}|^2 , \qquad (6)$$

where C is a normalization constant, containing cross-section per event, etc. The amplitudes $A_{\alpha\beta\lambda_1\lambda_2}$ can be expanded in terms of partial wave amplitudes $A^J_{\mu,\alpha\beta\lambda_1\lambda_2}$, with total spin J and helicity μ of the $p\bar{p}$ system in the t-channel reference frame:

$$A_{\alpha\beta\lambda_1\lambda_2}(M,t,\Omega) = \frac{1}{\sqrt{4\pi}} \sum_{J,\mu} (2J+1)^{1/2}\, D^{J*}_{\mu\lambda}(\phi,\cos\theta,-\phi)\, A^J_{\mu,\alpha\beta\lambda_1\lambda_2}(M,t) , \qquad (7)$$

where $D^J_{\mu\lambda}(\phi,\cos\theta,-\phi)$ are the rotation matrices, $\lambda \equiv \lambda_1 - \lambda_2$, $\Omega \equiv (\cos\theta, \phi)$.

The analysis was performed under the standard assumptions for resonance production by OPE with absorption (OPEA) corrections. Below are listed the assumptions for the production amplitudes based on a "Poor Man's Absorption Model" [11,12]:

i) Helicity amplitudes with nucleon spin flip in the s-channel helicity system dominate at our energies;

ii) Helicity amplitudes for production of the system with mass M and spin J are in phase except for an unobservable phase between natural and unnatural exchange;

iii) In the t-region analysed, the moments $\langle Y^L_m \rangle$ with $m \geq 2$ can be assumed to be zero. This entails the vanishing of all helicity amplitudes A^J_μ with $\mu \geq 2$ and equality $|A^J_-| = |A^J_+|$ for $\mu = 1$, where $A^J_\pm = (1/\sqrt{2})[A^J_\mu \pm (-1)^\mu A^J_{-\mu}]$ (indices λ_1, λ_2 are omitted);

iv) A^J_-/A^J_0 is a smooth function of M.

The above assumptions have been used for reaction (c) by Ochs [12], Estabrooks and Martin [13], and Hyams et al. [14], and for reaction (d) by Cohen et al. [15].

These assumptions have also been checked for these reactions using a polarized target experiment, which allowed for a model-independent analysis [16,17]. A systematic deviation has been found from assumptions (i) and (ii). This deviation, however, decreases with increasing mass and is of marginal significance already in the g(1690) region. Therefore we feel quite justified in using these assumptions in this analysis.

However, even with these assumptions, only an energy-dependent analysis is possible and a further parametrization is required. Data for the analysis are presented in terms of GJ moments averaged over the t-interval from t_{min} up to 0.3 GeV^2. (The relations between moments and amplitudes are given in the Appendix):

$$\left\langle Y_\mu^L(M)\right\rangle = \int_{t_{min}}^{0.3\ \mathrm{GeV}^2} \left\langle Y_\mu^L(M,t)\right\rangle \, dt \ .$$

Because of the dependence of t_{min} on the $p\bar{p}$ mass, it was necessary to specify a t-dependence of the amplitudes A_μ^J. The amplitudes A_μ^J were parametrized in terms of the OPE model:

$$A_0^J(M,t) = \frac{\sqrt{t}}{(t + m_\pi^2)} \sqrt{F_{DP}(t)}\ M/\sqrt{q^*}\ \langle\lambda_1\lambda_2|T^J(M)|0,0\rangle \tag{8}$$

$$A_-^J(M,t) = A_-^J(M) = C_A^J(M)\ M/\sqrt{q^*}\ T^J(M)\ , \tag{9}$$

where $\langle\lambda_1\lambda_2|T^J(M)|0,0\rangle \equiv T^J$ are, up to a normalization constant, the $\pi^+\pi^- \to p\bar{p}$ partial wave amplitudes at c.m. energy M. The data are not sensitive enough to test a t-dependence of the A_-^J amplitudes and a weak dependence on t of these amplitudes was neglected.

The relation between amplitudes A_-^J and A_0^J as a function of mass were parametrized using the phenomenological formula from ref. [18]:

$$C_A^J(M) = \sqrt{J(J+1)}\ \frac{C_0}{1 + C_1 M^2} \tag{10}$$

where, according to assumption (ii), C_0 and C_1 are real parameters. Because we

fit only a mass dependence of the moments, this parametrization of the amplitudes A_-^J as a function of t affects only the parameters C_0 and C_1 in formula (10).

The above parametrization cannot be applied to the lowest mass region, because of apparently different t behaviour. Thus the mass region below 1.975 was excluded from the further analysis.

The assumption of OPE restricts the quantum numbers of the $p\bar{p}$ system to natural spin-parity states: $J^{PC} = 0^{++}, 1^{--}, 2^{++}, \ldots$. States with even spin have isospin I = 0, and states with odd spin have isospin I = 1. Since many partial waves evidently contribute, resonance parameters extracted from the fit depend on the parametrization of T^J amplitudes. In our fits we tried several combinations of conventional parametrizations: resonance and a slowly varying background (polynomial parametrization).

In the fits the resonances were parametrized in the following form:

$$\langle \tfrac{1}{2}, \tfrac{1}{2} | T^J | 0,0 \rangle = \frac{a_J M_R \Gamma_R}{M^2 - M_R^2 - iM_R\Gamma_R}$$
$$\langle \tfrac{1}{2}, -\tfrac{1}{2} | T^J | 0,0 \rangle = \frac{b_J M_R \Gamma_R}{M^2 - M_R^2 - iM_R\Gamma_R} \quad . \tag{11}$$

Parameters a_J and b_J were set to be real. In the simplest approximation Γ was assumed to be independent of the angular momentum:

$$\Gamma_R = \Gamma_0 q/q_R$$
$$q_R = q(M = M_R) \quad . \tag{12}$$

A modification of Γ_R by Blatt-Weisskopf coefficients [19] did not improve the quality of the fit. Apart from this, a calculation of these coefficients for high values of L is a very time-consuming procedure, and finally the mass dependence of $\Gamma(M)$ was as in eq. (12). Fits were performed using the minimization program MINUIT [20]. In the first step, the mass region between 1.975 and 2.55 GeV was fitted, assuming one resonance in the 1^-, 2^+, 3^-, 4^+, 5^- waves (four parameters per wave) and a non-resonant background in the 0^+ wave:

$$\begin{aligned} \text{Re}\ (\langle \tfrac{1}{2},\tfrac{1}{2}|T^0|0,0\rangle) &= a_1 + b_1 M + c_1 M^2 \\ \text{Im}\ (\langle \tfrac{1}{2},\tfrac{1}{2}|T^0|0,0\rangle) &= a_2 + b_2 M + c_2 M^2 \ . \end{aligned} \tag{13}$$

The mass of the resonance in the 1^- wave was found to be always below the analysed region and in the next step a non-resonant background in this wave was assumed:

$$\begin{aligned} \text{Re}\ (\langle \lambda_1,\lambda_2|T^1|0,0\rangle) &= A_1 + B_1 M \\ \text{Im}\ (\langle \lambda_1,\lambda_2|T^1|0,0\rangle) &= A_2 + B_2 M \ . \end{aligned} \tag{14}$$

Parameters of resonances obtained in this fit are listed in Table 2 (numbers in brackets). The χ^2 per degree of freedom (p.d.f.) was 2.6 with the main contribution from a few data points with mass around 2 GeV. Figure 8 shows the χ^2 distribution as a function of mass. A significant improvement of the fit was obtained when two coherent spin 4 resonances were allowed. A good fit with a second resonance at a mass of 2.04 GeV was found. Owing to its mass and width, we attribute this state to the h meson on the leading trajectory. The small contribution of this state improves the value of χ^2 p.d.f. from 2.6 to 1.8, without essentially changing the parameters of the other resonances. An addition of a second resonance in any lower partial waves instead of the h meson did not improve the fit.

Extension of the analysis to higher masses, up to 2.75 GeV, with the above parametrization increased the value of χ^2 p.d.f. to 2.2 with a bad description of the data at a mass around 2.7 GeV as can be seen from the χ^2 distribution in fig. 9. Once the position of the highest resonance (spin 5 at 2.45 GeV) is passed, the model used predicts a decreasing forward-backward asymmetry and all the contributions of the interference terms and intensities in the relevant moments should rapidly decrease. In order to describe the data correctly one needs at least a rising background in some partial waves or a further resonance with a mass above 2.5 GeV. Adding smooth background terms to the various partial waves did not significantly improve the description of the moments above 2.5 GeV (for example, as shown in ref. [2]), while a satisfactory description of the high mass data was obtained by the addition of a resonance in a 6^+ wave with the resulting χ^2 p.d.f. = = 1.75. There is a very weak signal for this state in the $\langle Y_0^{12} \rangle$ moment, but a

very small amount of this resonance significantly improves the description of the lower moments as they contain the interference terms of the spin 6 with the other waves. It should be emphasized that, since the parameters of the lower partial waves are essentially determined by fitting the lower mass region, the wave 6^+ enters the moments equation in a well-defined way.

In our fits, other parametrizations for the background in the waves 0^+, 1^- were also tried; for instance, amplitudes T^1 and T^0 were expressed as explicit functions of q and q^* but it did not change the resonance parameters nor the value of χ^2. Further details of the fits are discussed in ref. [21].

Fits were primarily made to the $\langle Y_0^L \rangle$ moments. After determining the parameters of A_0^J amplitudes, the moments $\langle Y_1^L \rangle$ were included in the fit, mainly to determine the values of parameters C_0 and C_1. The final fit results for the mass range between 1.975 and 2.75 GeV with parametrizations defined by eqs. (8) to (14) are listed in table 2. The results are also indicated as solid lines in figs. 4-6. The final fit to the mass spectrum together with the contribution of the background waves 0^+ and 1^- are shown in fig. 10.

6. DISCUSSION OF RESULTS

Figure 11 shows the positions of the resonances on the Chew-Frautschi plot, together with results of the other $p\bar{p}$ experiments and established states coupling to the $\pi\pi$ channel. Assuming that the resonances $3^-(2.11)$, $4^+(2.38)$, $5^-(2.45)$, $6^+(2.71)$ lie on the same degenerated daughter trajectory, we can fit the parameters for this trajectory. We obtain a trajectory with a slope of 1.10 ± 0.03 and an intercept of -1.95 ± 0.2. With these parameters we predict the following states: $0^+(1330)$, $1^-(1630)$, $2^+(1890)$. The first two states can be reconciled with $\varepsilon(1300)$ and $\rho'(1600)$ resonances. The resonances $3^-(2.11)$ and $4^+(2.38)$ coincide with the resonances T(M = 2192 ± 10 MeV, Γ = 150 ± 50 MeV) and U(M = 2350 ± 25 MeV, $\Gamma \sim 200$ MeV) listed in the Review of Particle Properties [22]. The positions of the resonances 3^-, 4^+, 5^- of our analysis are consistent with those obtained by Carter et al. [23] in a recent analysis of the reactions

$p\bar{p} \to \pi^+\pi^-$ and $\bar{p}p_\uparrow \to \pi^+\pi^-$ in the c.m. energy range between 2.02 and 2.58 GeV, despite considerable differences in assumptions made about non-resonant background and Breit-Wigner parametrizations.

The main difference between the two analyses is the parametrization of the 2^+ wave. In ref. [23] a non-resonant background in this wave is assumed. The mass of the resonance $2^+(2.18)$ obtained in our fit is higher than the mass of the resonance $3^-(2.11)$ and the resonance 2^+ does not belong to the same trajectory as the resonances 3^-, 4^+, 5^-, 6^+. A confirmation of this state comes from the analysis of the reaction $p\bar{p} \to 2\pi^0$ [24], allowing only I = 0 even spin states. In this analysis two resonances $2^+(2.15)$ and $4^+(2.33)$ were found. Our analysis also differs by the addition of a second resonance in the 4^+ wave (h meson), which was earlier observed in decays into K^+K^- pairs [26] and into $2\pi^0$ [27]. Mass and width obtained for this resonance agree very well with those listed in the Review of Particle Properties [22], which are 2040 ± 20 MeV and 193 ± 50 MeV, respectively. Using the cross-section for the h decay into K^+K^- of $\sigma = 0.35 \pm 0.04$ μb, we estimate a branching ratio ($1.95 < m < 2.4$ GeV):

$$\sigma(h \to p\bar{p})/\sigma(h \to K^+K^-) = 0.17 \pm 0.04 \ ,$$

but this result is strongly dependent on the parametrization of the background.

Our data extend to a higher mass region compared with other experiments, so we cannot expect any confirmation of the meson $6^+(2.71)$.

The values of the parameters C_0 and C_1 are consistent with those obtained for reactions (c) and (d). This very simple parametrization in general reproduces the most prominent features of the $\langle Y_1^L \rangle$ moments.

We conclude finally that reaction (a) is also a good source of information about the reaction $p\bar{p} \to \pi^+\pi^-$, owing to some experimental advantages such as simpler normalization and a non-zero acceptance in the full range of decay angles over a wide mass range.

REFERENCES

[1] A.J.G. Hey and D. Morgan, Meson spectroscopy, Rutherford Laboratory, Chilton, Preprint RL-77-060/A (1977).

[2] J. Meissburger, Thesis, University of Munich, Max Planck Institute, Report MPI-PAE/Exp.E1.48.

[3] B. Hyams et al., Phys. Lett. 39B (1972) 563.

[4] E. Eisenhandler et al., Phys. Lett. 47B (1973) 532.

[5] A.A. Carter et al., Nucl. Phys. B127 (1977) 202.

[6] G. Hentschel, Thesis, University of Munich, Max Planck Institute, Report MPI-PAE/Exp.E1.56.

[7] G. Wolf, Phys. Rev. 182 (1966) 1538.

[8] H.P. Dürr and H. Pilkuhn, Nuovo Cimento 40 (1965) 897.

[9] G.F. Chew and F.E. Low, Phys. Rev. 113 (1959) 1640.

[10] G. Grayer et al., Nucl. Phys. B75 (1974) 189.

[11] B. Hyams et al., Nucl. Phys. B64 (1973) 134.

[12] W. Ochs, Thesis, University of Munich, 1973.

[13] P. Estabrooks and A.D. Martin, Nucl. Phys. B79 (1974) 301.

[14] B. Hyams et al., Nucl. Phys. B64 (1973) 134.

[15] D. Cohen et al., $K\bar{K}$ amplitude analysis, Argonne National Laboratory, Preprint ANL-HEP-CP-77-37.

[16] H. Becker et al., Nucl. Phys. B150 (1979) 301.

[17] H. Becker et al., Nucl. Phys. B151 (1979) 46.

[18] P. Estabrooks and A.D. Martin, $\pi\pi$ partial wave analysis from 0.6 to 1.8 GeV Department of Physics, University of Durham, Preprint (March 1975).

[19] J. Blatt and V. Weisskopf, Theoretical nuclear physics (Wiley, New York, 1952), p. 361.

[20] F. James and M. Roos, Comput. Phys. Commun. 10 (1975) 343.

[21] M. Rozanska, Thesis, Institute of Nuclear Physics, Cracow, 1979.

[22] Particle Data Group, Review of Particle Properties, 1978.

[23] A.A. Carter et al., Phys. Lett. 67B (1977) 117.

[24] R.S. Dulude et al., submitted to the IVth European Antiproton Symposium, Barr, 1978.

[25] A. Donnachie and P.R. Thomas, Nuovo Cimento Letters 7 (1975) 285.

[26] W. Blum et al., Phys. Lett. 57B (1975) 403.

[27] W.D. Apel et al, Phys. Lett. 57B (1975) 398.

Table 1

Numbers of events and background contributions

p_{lab}	18.8 GeV	18.4 GeV
No. of events	10,700	30,500
$\pi^+\pi^-n$ background	1%	$\leq$ 0.5%
K^+K^-n background	4%	$\sim$ 1%
$p\bar{p}(n\pi^0)$ background	3%	$\leq$ 2%

Table 2

Results of the fit to the $\bar{p}p$ mass spectrum and moments

J^P	M (MeV)	Γ (MeV)	a_J/b_3	b_J/b_3	Fraction of total mass spectrum (%)
2^+	2180 ± 10	270 ± 10	-0.86 ± 0.04	-0.51 ± 0.02	19.4 ± 0.7
	(2150 ± 10)	(260 ± 10)	(-1.30 ± 0.04)	(-0.60 ± 0.03)	(27.0 ± 0.6)
3^-	2110 ± 10	190 ± 10	0.36 ± 0.01	1	14.7 ± 0.5
	(2080 ± 10)	(190 ± 15)	(0.22 ± 0.04)	(1)	(9.6 ± 0.5)
4^+(h)	2040 ± 10	140 ± 15	-0.36 ± 0.02	0.02 ± 0.01	15.0 ± 0.5
4^+	2380 ± 10	380 ± 20	0.69 ± 0.02	0.24 ± 0.01	
	(2360 ± 10)	(430 ± 30)	(0.69 ± 0.04)	(0.27 ± 0.03)	(11.3 ± 0.6)
5^-	2450 ± 10	280 ± 20	0.11 ± 0.01	0.64 ± 0.04	10.4 ± 0.4
	(2440 ± 10)	(310 ± 20)	(0.20 ± 0.03)	(0.80 ± 0.03)	(11.2 ± 0.5)
6^+	2710 ± 20	170 ± 40	0.28 ± 0.04	-0.02 ± 0.03	1.5 ± 0.2
0^+	$a_1 = -0.58 \pm 0.09$ $b_1 = -1.76 \pm 0.02$ $c_1 = 0.77 \pm 0.02$ $a_2 = -1.77 \pm 0.11$ $b_2 = 0.31 \pm 0.01$ $c_2 = 0.16 \pm 0.02$				15.0 ± 1.0
1^-	$\lambda_1 = \lambda_2$	$A_1 = 0.03 \pm 0.04$ $B_1 = 0.04 \pm 0.01$ $A_2 = -0.55 \pm 0.02$ $B_2 = 0.09 \pm 0.01$			24.0 ± 2.0
	$\lambda_1 = -\lambda_2$	$A_1 = 1.16 \pm 0.04$ $B_1 = 0.14 \pm 0.01$ $A_2 = -1.10 \pm 0.02$ $B_2 = 0.10 \pm 0.04$			

$C_0 = 0.19 \pm 0.04$, $C_1 = -1.65 \pm 0.03$.

Values in brackets denote results of the fit in the mass range 1.95-2.55 GeV with only one 4^+ state.

Figure captions

Fig. 1 : $p\bar{p}$: effective mass spectrum for $t < 0.3$ GeV^2.

$\blacklozenge$: measured in reaction (a). σ(1 event) = 0.08 ± 0.01 nb.

ϕ: OPE prediction from annihilation data $p\bar{p} \to \pi^+\pi^-$.

Fig. 2 : Geometrical acceptance for an isotropically decaying $p\bar{p}$ system.

Fig. 3 : Corrected $d\sigma/dt$ cross-sections. The continuous curves are OPE predictions.

Figs. 4-6 : Unnormalized $\langle Y_0^L \rangle$ and $\langle Y_1^L \rangle$ moments of the angular distribution in the Gottfried-Jackson frame. The curves are the results of the final fit.

Fig. 7 : $d\sigma/d\cos\theta$ of ref. [5]. The continuous curves are calculated from $\langle Y_0^L \rangle$ moments measured in reaction (a).

Fig. 8 : The χ^2 per data point as a function of $p\bar{p}$ mass.

Dashed line: fit without a second 4^- meson.

Full line: fit with a second 4^- meson.

Fig. 9 : The χ^2 per data point as a function of $p\bar{p}$ mass.

Dashed line: fit without resonance 6^+;

Full line: fit with resonance 6^+.

Fig. 10 : Results of the fit for the $p\bar{p}$ mass spectrum for $t < 0.3$ GeV^2. The solid lines show the fitted mass spectrum and the contributions of the 0^+ and 1^- waves.

Fig. 11 : Resonance positions in the Chew-Frautschi plot.

APPENDIX

RELATIONS BETWEEN MOMENTS AND AMPLITUDES

In order to express the moments $\langle Y_\mu^L \rangle$ in terms of amplitudes we substitute eq. (7) in eq. (6):

$$\frac{d^4\sigma}{dtdMd\Omega} = \frac{C}{4\pi} \sum_{\substack{\alpha\beta \\ \lambda_1\lambda_2}} \sum_{\substack{j\mu \\ j'\mu'}} (2J' + 1)^{1/2}(2J + 1)^{1/2} D^{J*}_{\mu\lambda}(\Omega)\, D^{J'}_{\mu'\lambda}(\Omega)\, A^J_{\mu,\alpha\beta\lambda_1\lambda_2}\, A^{J'*}_{\mu',\alpha\beta\lambda_1\lambda_2} \cdot \tag{A.1}$$

Expanding products $D^{J*}_{\mu\lambda}(\Omega)D^{J'}_{\mu'\lambda}(\Omega)$ in the Clebsch-Gordan series:

$$D^{J*}_{\mu\lambda}(\Omega)\, D^{J'}_{\mu'\lambda}(\Omega) = \sum_L \langle J'J\mu' - \mu | L\mu''\rangle \langle J'J\lambda - \lambda | L0\rangle (-1)^{\mu-\lambda}\, D^L_{\mu''0}(\Omega)$$

and using the relation

$$D^L_{\mu 0}(\Omega) = \sqrt{\frac{4\pi}{2L + 1}}\, Y^{L*}_\mu(\Omega) \ ,$$

we obtain

$$\frac{d^4\sigma}{dtdMd\Omega} = C \sum_{\substack{\alpha\beta \\ \lambda_1\lambda_2}} \sum_{\substack{J\mu \\ J'\mu'}} \sum_L \sqrt{\frac{(2J + 1)(2J' + 1)}{4\pi(2L + 1)}}\, \langle J'J,\mu' - \mu | L\mu''\rangle \langle J'J\lambda - \lambda | L0\rangle \times$$

$$\times (-1)^{\mu-\lambda}\, Y^{L*}_{\mu''}(\Omega)\, A^J_{\mu,\alpha\beta\lambda_1\lambda_2}\, A^{J'*}_{\mu',\alpha\beta\lambda_1\lambda_2} \cdot \tag{A.2}$$

Both sides of eq. (A.2) can be multiplied by $Y^{L'}_{\mu''}$ and integrated over Ω. This together with orthonormality of spherical harmonics gives the required relation:

$$N\langle Y^L_{\mu''}\rangle = \sum_{\substack{\alpha\beta \\ \lambda_1\lambda_2}} \sum_{\substack{J\mu \\ J'\mu'}} \sqrt{\frac{(2J + 1)(2J' + 1)}{4\pi(2L + 1)}}\, \langle J'J\mu' - \mu | L\mu''\rangle \langle J'J\lambda - \lambda | L0\rangle (-1)^{\mu-\lambda} \times$$

$$\times A^J_{\mu,\alpha\beta\lambda_1\lambda_2}\, A^{J'*}_{\mu',\alpha\beta\lambda_1\lambda_2} \cdot$$

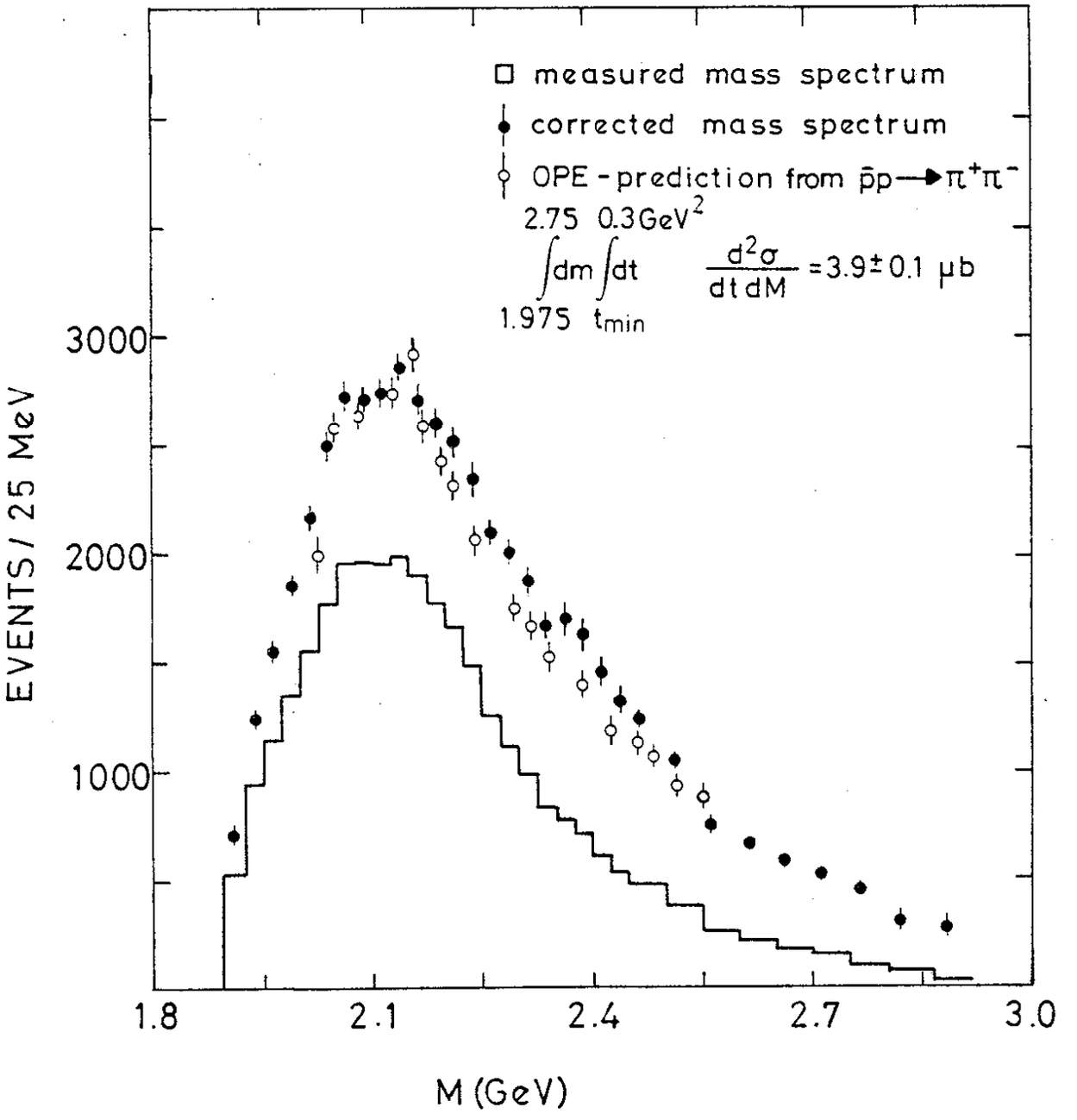
measured mass spectrum
corrected mass spectrum
OPE - prediction from $\bar{p}p \rightarrow \pi^+\pi^-$
$\int_{1.975}^{2.75} dm \int_{t_{min}}^{0.3\,GeV^2} dt \quad \frac{d^2\sigma}{dt\,dM} = 3.9 \pm 0.1\ \mu b$
EVENTS / 25 MeV
3000
2000
1000
1.8
2.1
2.4
2.7
3.0
M (GeV)

Fig. 1

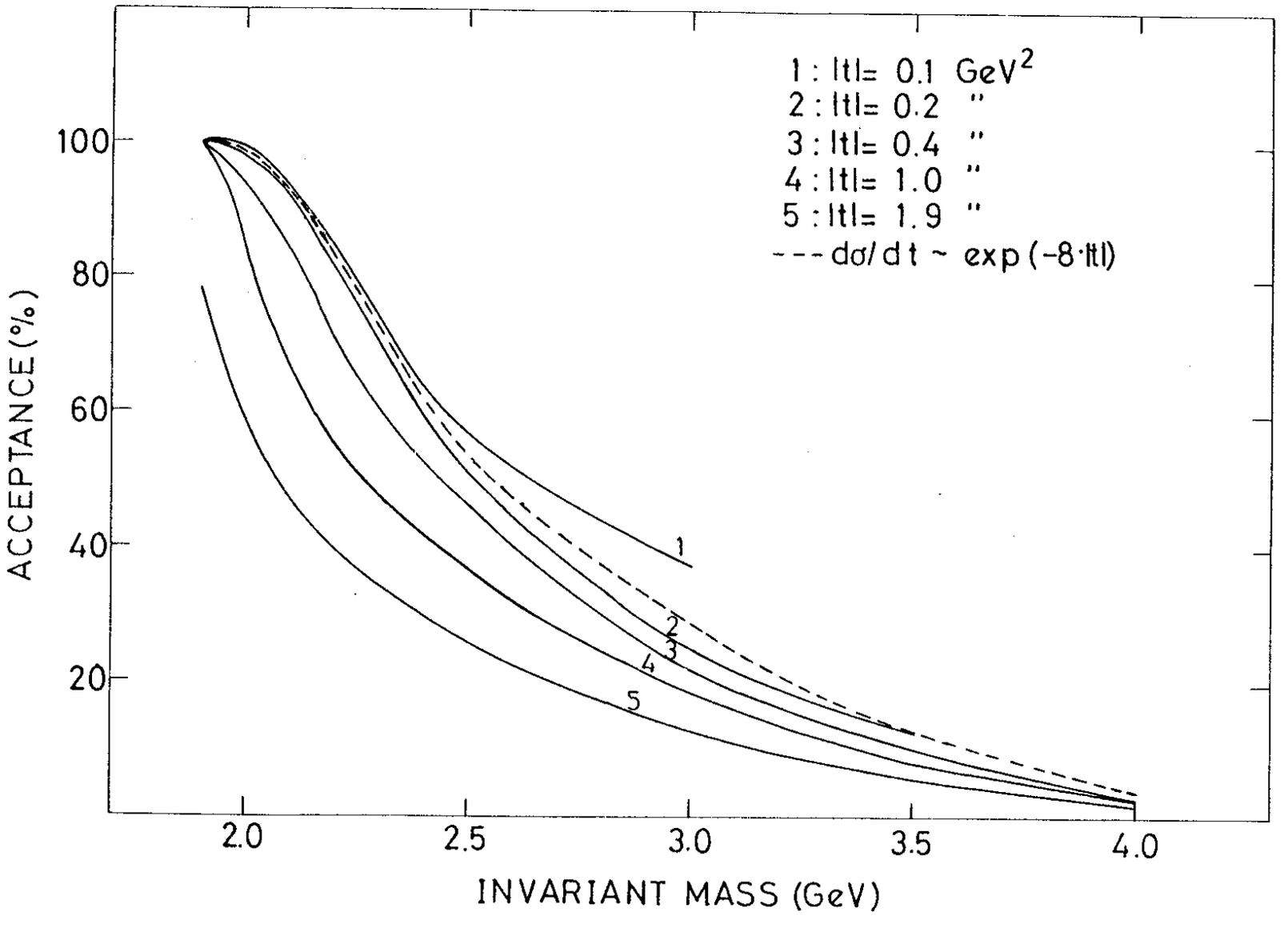
1 : |t|= 0.1 GeV²
2 : |t|= 0.2 "
3 : |t|= 0.4 "
4 : |t|= 1.0 "
5 : |t|= 1.9 "
--- dσ/dt ~ exp(-8·|t|)
ACCEPTANCE (%)
100
80
60
40
20
2.0
2.5
3.0
3.5
4.0
INVARIANT MASS (GeV)
1
2
3
4
5

Fig. 2

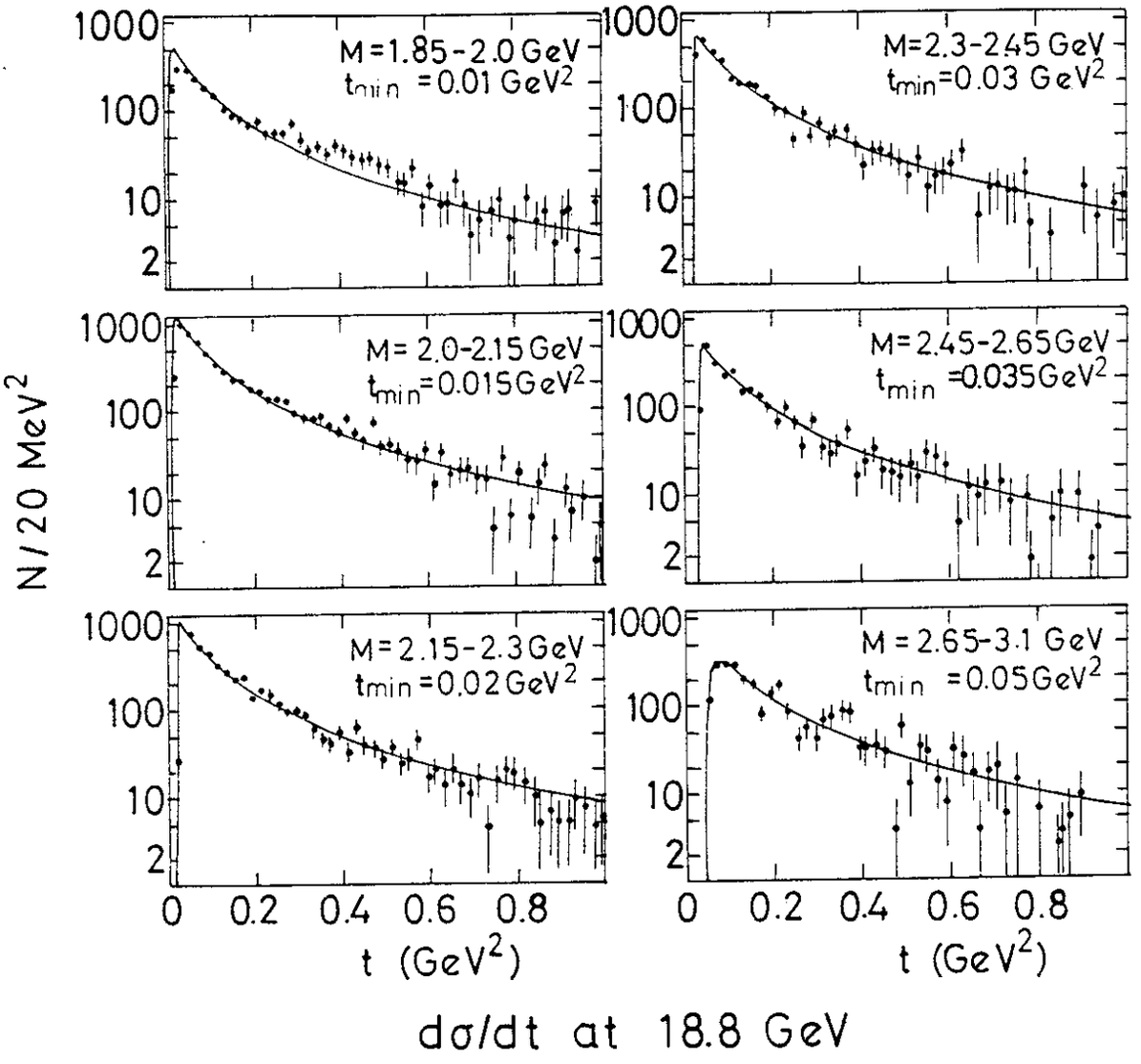
M=1.85-2.0 GeV
tmin =0.01 GeV2
M=2.3-2.45 GeV
tmin=0.03 GeV2
M= 2.0-2.15 GeV
tmin=0.015GeV2
M=2.45-2.65GeV
tmin =0.035GeV2
M=2.15-2.3GeV
tmin =0.02GeV2
M=2.65-3.1 GeV
tmin =0.05GeV2
1000
100
10
2
0
0.2
0.4
0.6
0.8
t (GeV2)
N/20 MeV2
dσ/dt at 18.8 GeV

Fig. 3

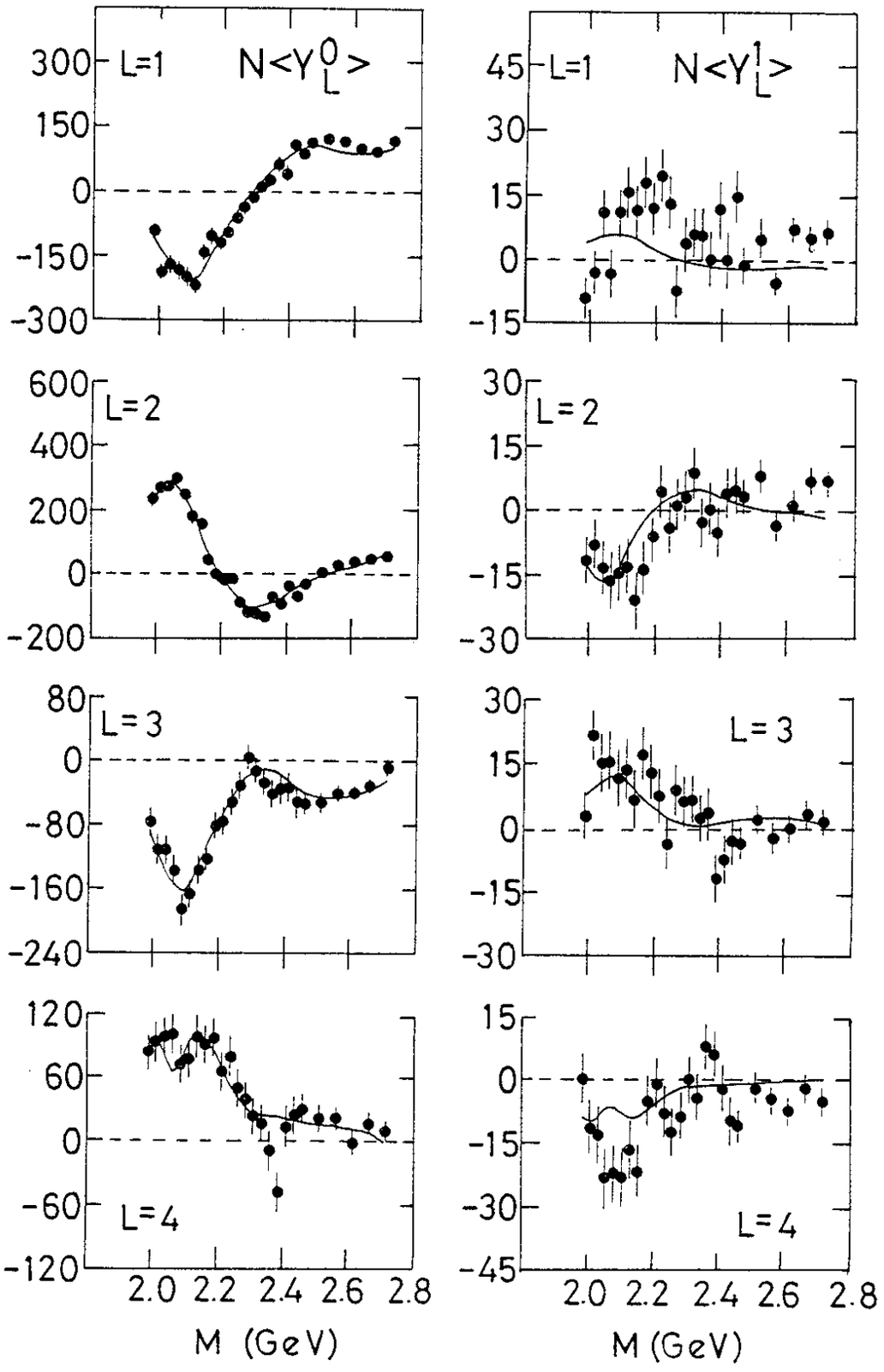
L=1
$N\langle Y_L^0 \rangle$
300
150
0
-150
-300
L=1
$N\langle Y_L^1 \rangle$
45
30
15
0
-15
600
400
200
0
-200
L=2
30
15
0
-15
-30
L=2
80
0
-80
-160
-240
L=3
30
15
0
-15
-30
L=3
120
60
0
-60
-120
L=4
15
0
-15
-30
-45
L=4
2.0 2.2 2.4 2.6 2.8
M (GeV)
2.0 2.2 2.4 2.6 2.8
M (GeV)

Fig. 4

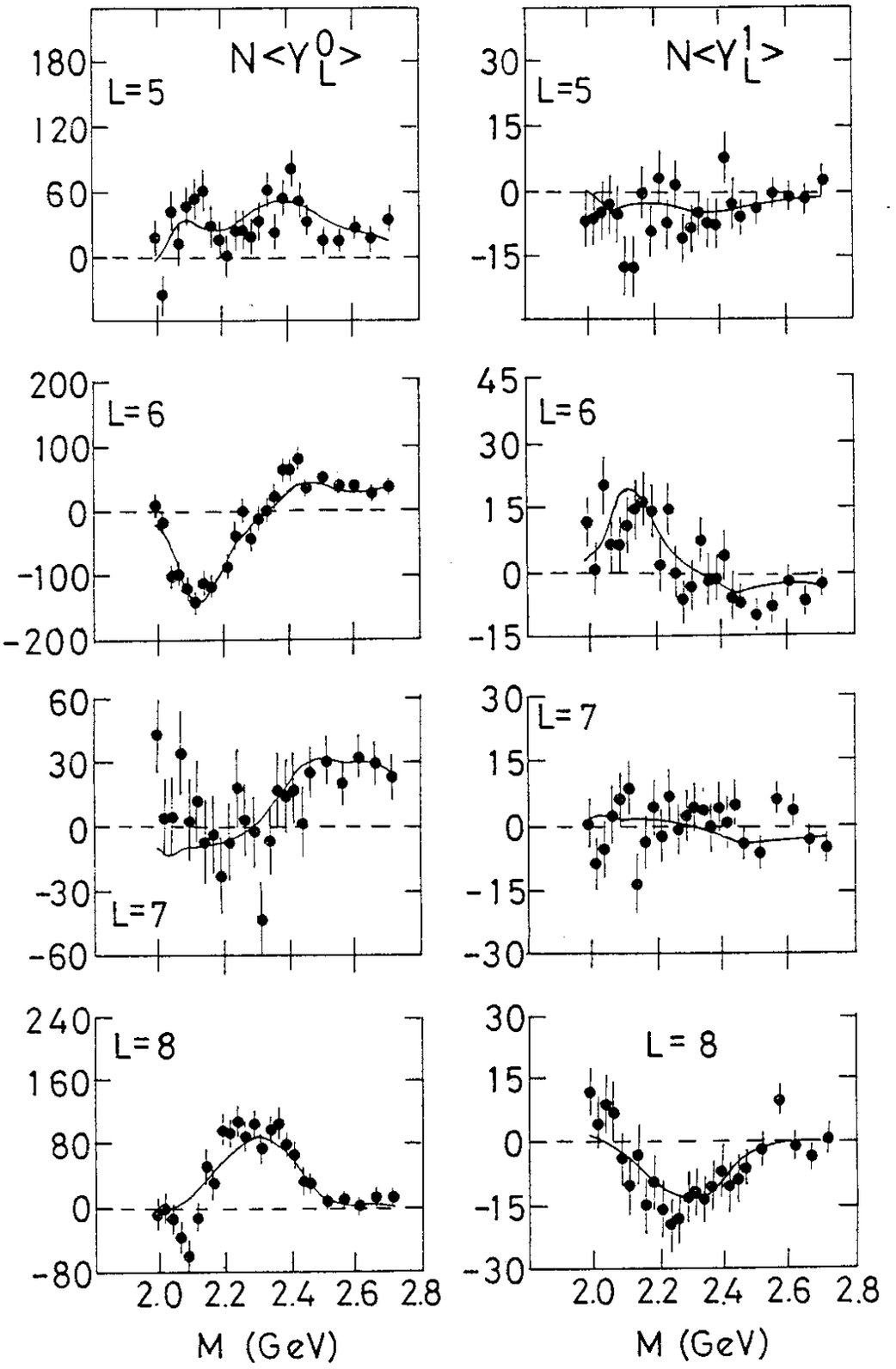
N<Y^0_L>
N<Y^1_L>
L=5
L=6
L=7
L=8
180
120
60
0
30
15
-15
200
100
-100
-200
45
-30
240
160
80
-80
2.0
2.2
2.4
2.6
2.8
M (GeV)

Fig. 5

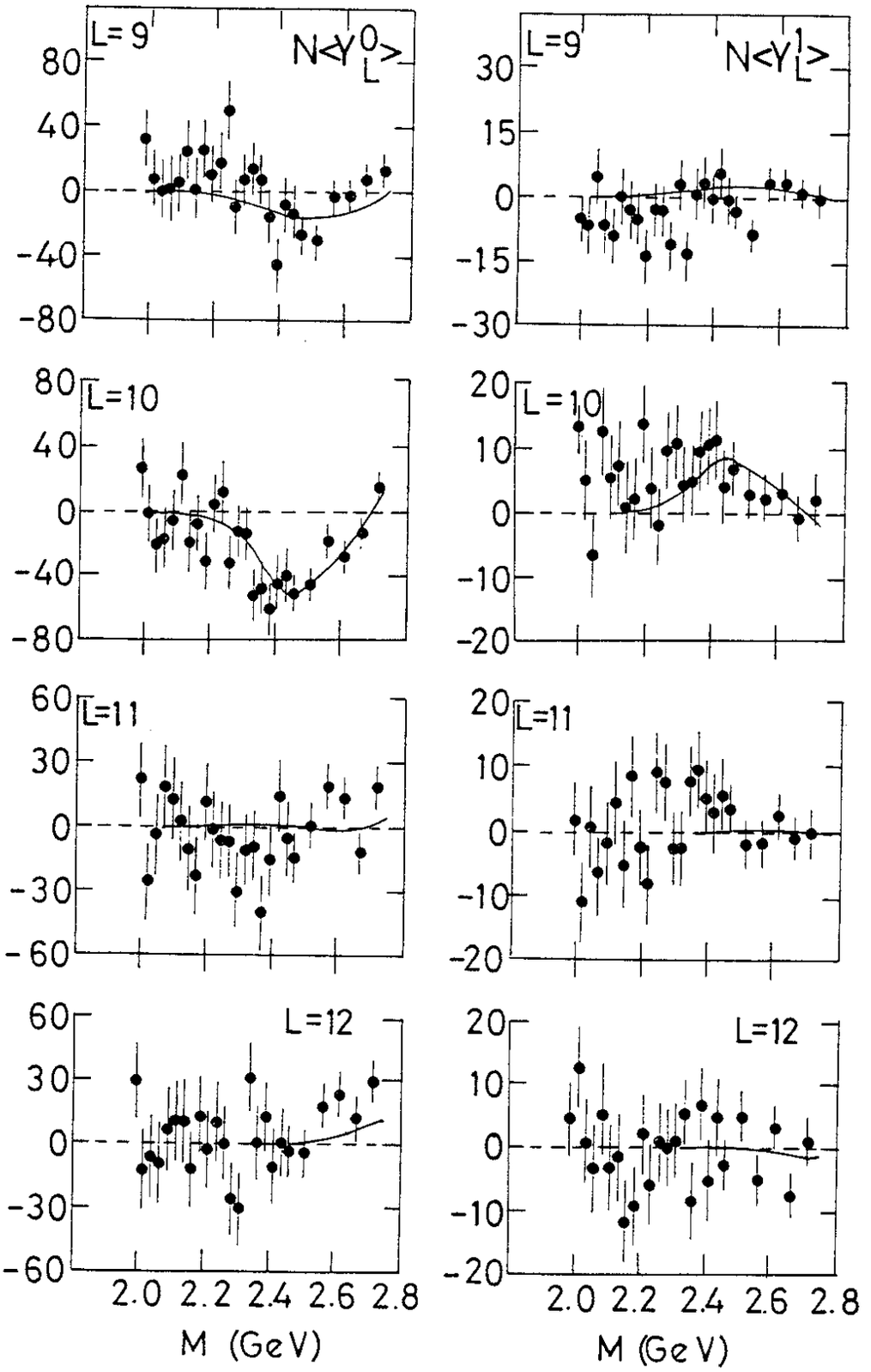

Fig. 6

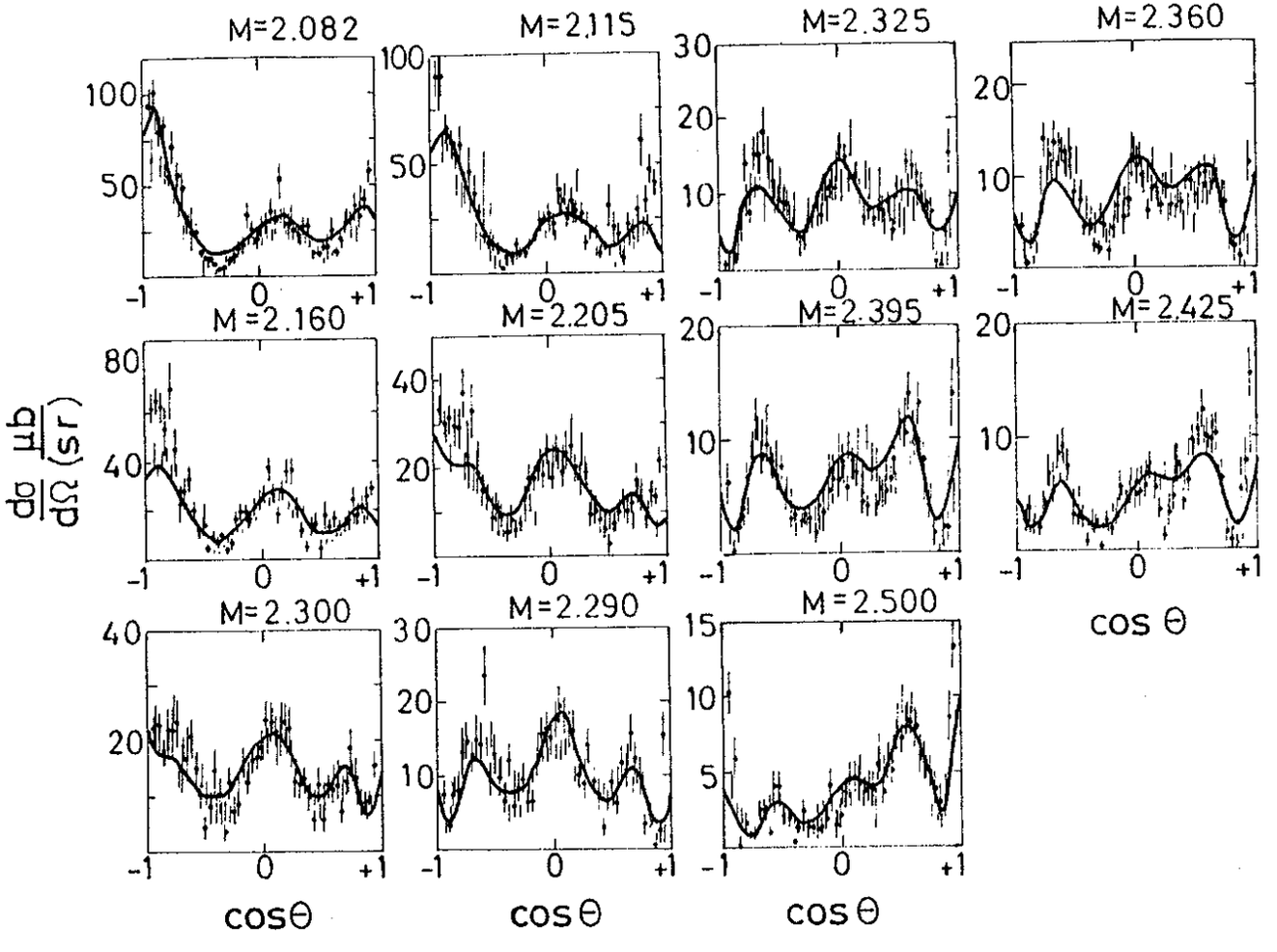
M=2.082
M=2.115
M=2.325
M=2.360
M=2.160
M=2.205
M=2.395
M=2.425
M=2.300
M=2.290
M=2.500
dσ/dΩ μb/sr
cos Θ
cos Θ
cos Θ
cos Θ

Fig. 7

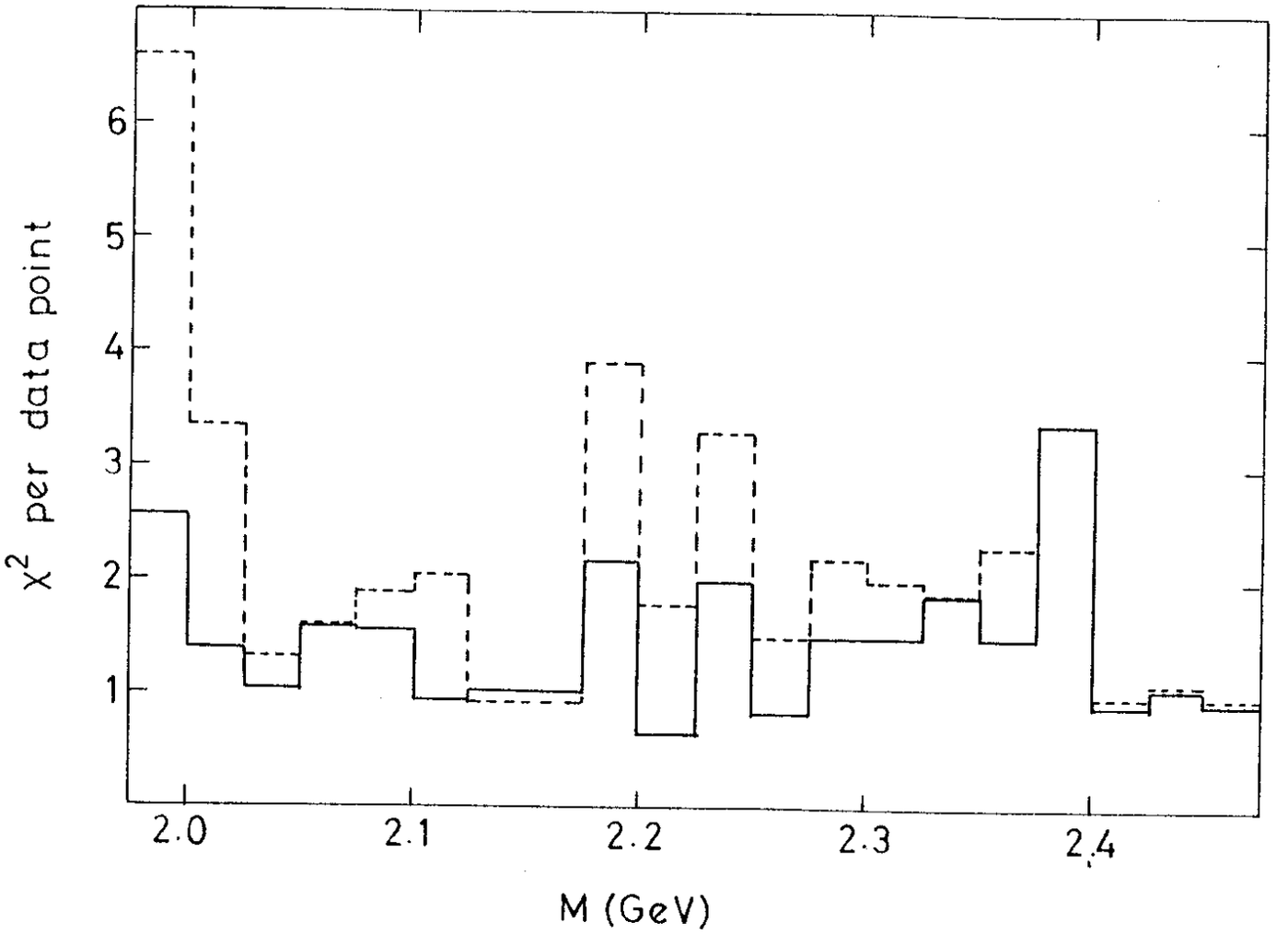

Fig. 8

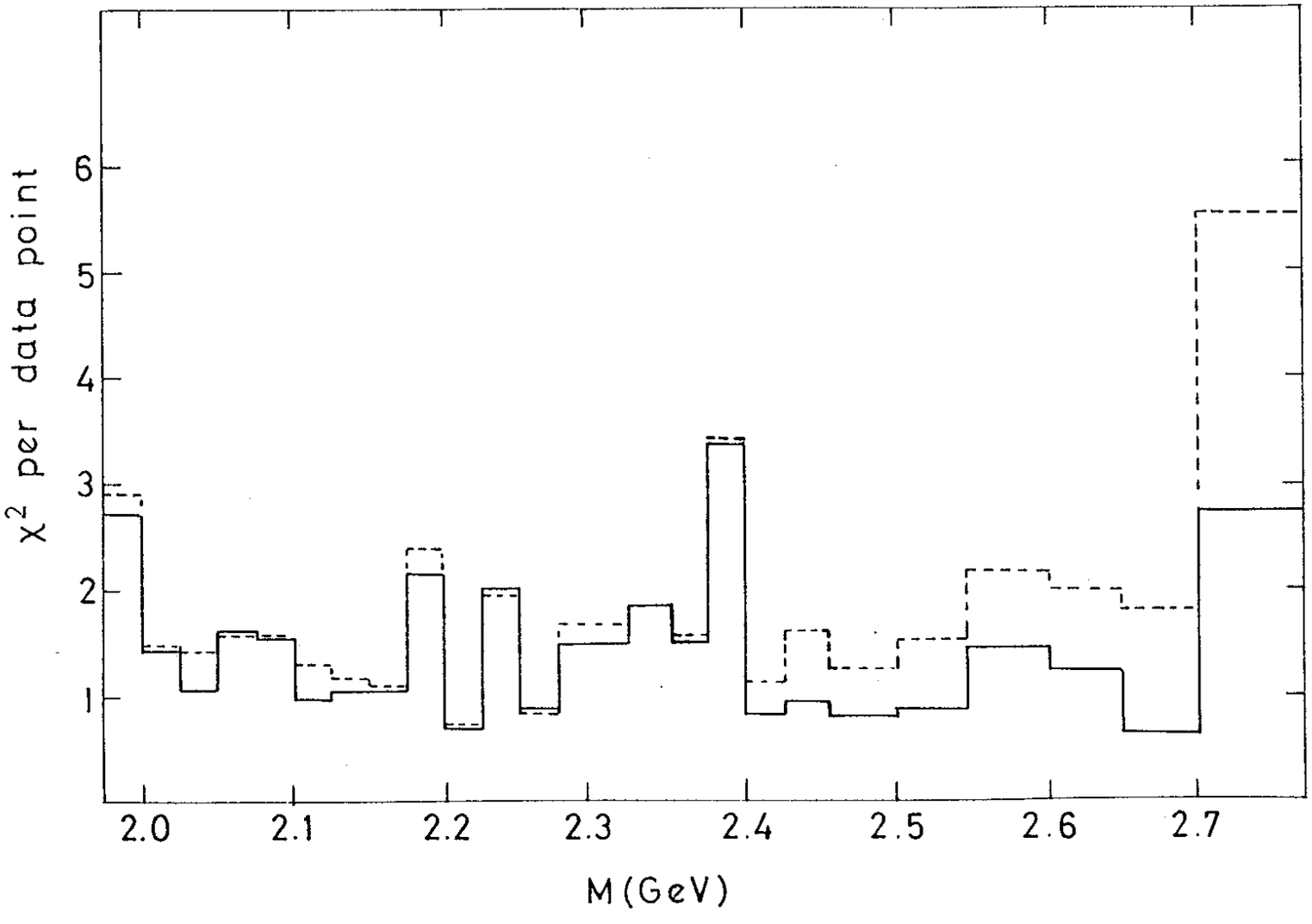

Fig. 9

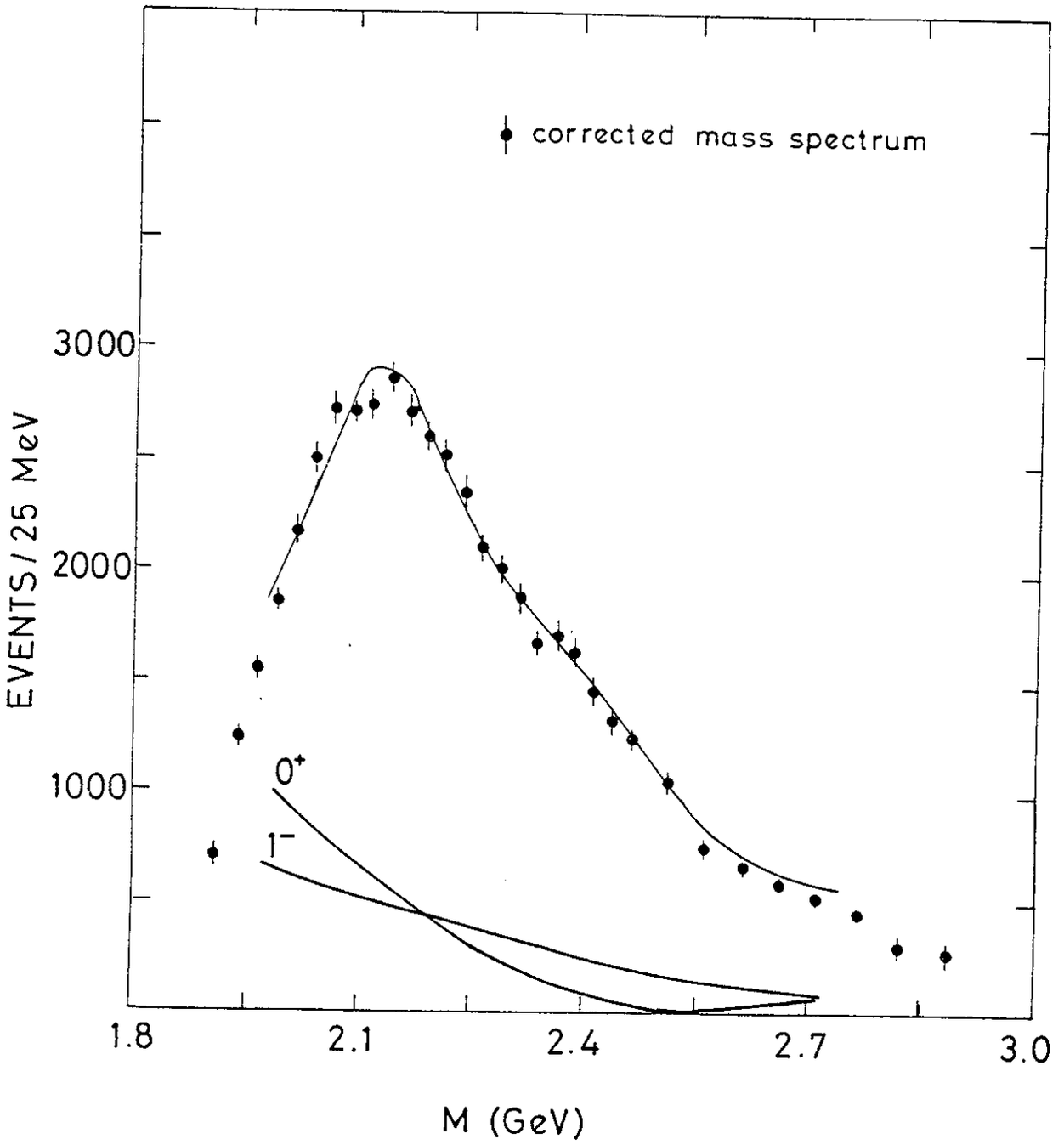
corrected mass spectrum
EVENTS / 25 MeV
3000
2000
1000
0+
1−
1.8
2.1
2.4
2.7
3.0
M (GeV)

Fig. 10

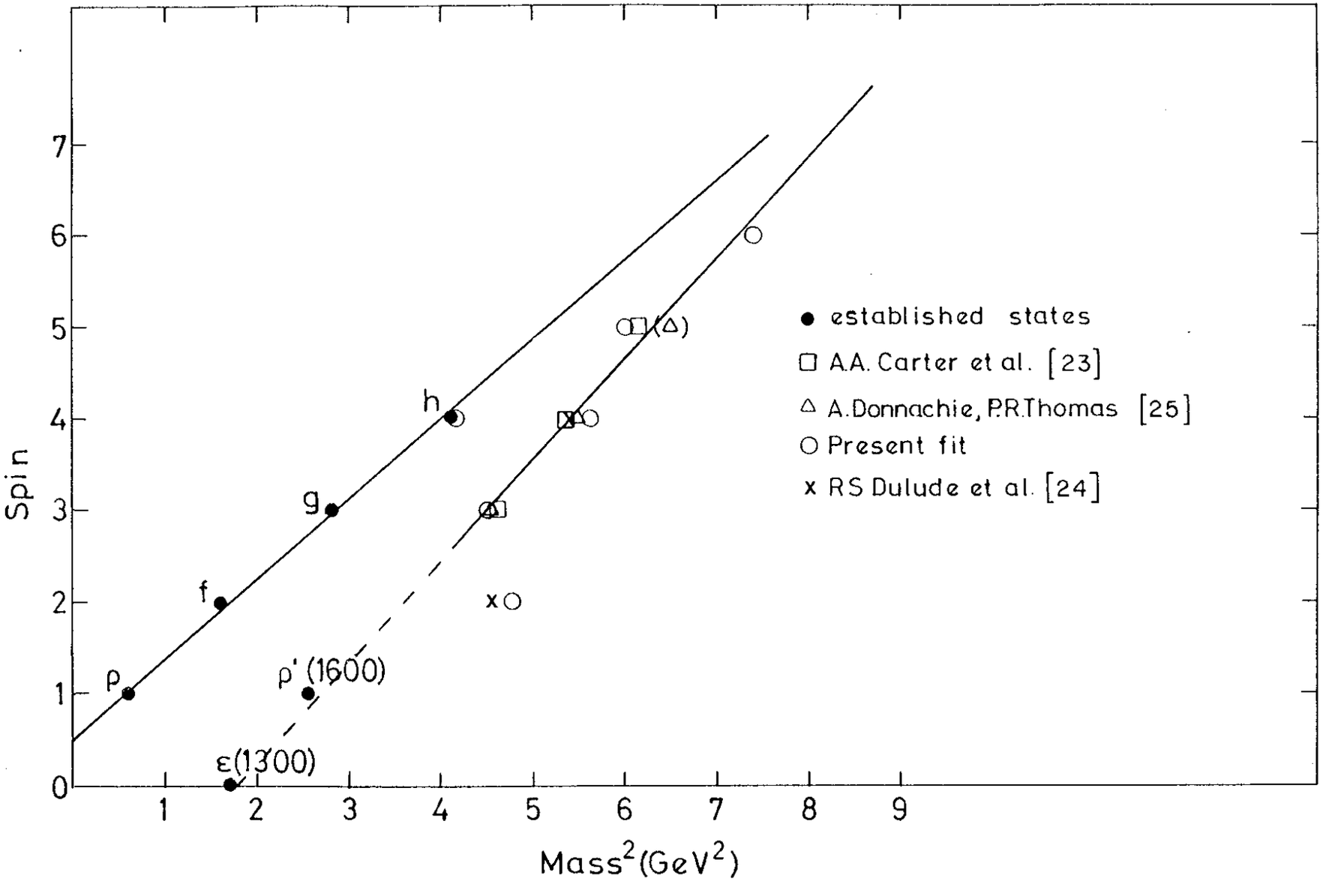
Spin
Mass^2(GeV^2)
0
1
2
3
4
5
6
7
8
9
ρ
f
g
h
ρ' (1600)
ε(1300)
(Δ)
x
● established states
□ A.A. Carter et al. [23]
△ A.Donnachie, P.R.Thomas [25]
○ Present fit
x RS Dulude et al. [24]

Fig. 11